

Rhodium-Phosphoramidite Catalyzed Alkene Hydroacylation: Mechanism and Octaketide Natural Product Synthesis

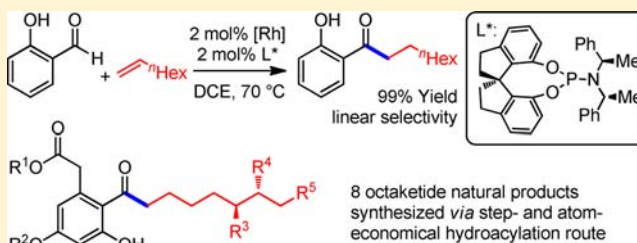
Max von Delius,[†] Christine M. Le,[†] and Vy M. Dong^{*,†,‡}

[†]Department of Chemistry, University of Toronto, 80 St. George Street, Toronto, Ontario M5S 3H6, Canada

[‡]Department of Chemistry, University of California, Irvine, California 92697-2025, United States

S Supporting Information

ABSTRACT: We describe a method that allows salicylaldehyde derivatives to be coupled with a wide range of unactivated alkenes at catalyst loadings as low as 2 mol %. A chiral phosphoramidite ligand and the precise stoichiometry of heterogeneous base are key for high catalytic activity and linear regioselectivity. This protocol was applied in the atom- and step-economical synthesis of eight biologically active octaketide natural products, including anticancer drug candidate cytosporone B. Mechanistic studies provide insight on parameters affecting decarbonylation, a side reaction that limits the turnover number for catalytic hydroacylation. Deuterium labeling studies show that branched hydride insertion is fully reversible, whereas linear hydride insertion is largely irreversible and turnover-limiting. We propose that ligand (*R_w*,*R_r*)-SIPHOS-PE effectively suppresses decarbonylation, and helps favor a turnover-limiting insertion, by lowering the barrier for reductive elimination in the linear-selective pathway. Together, these factors enable high reactivity and regioselectivity.



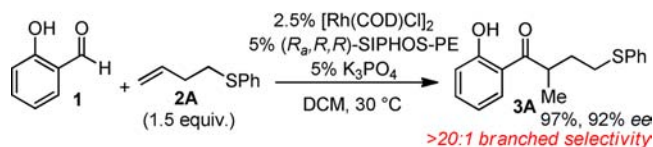
INTRODUCTION

Although alkene hydroacylation¹ is a conceptually ideal way to prepare ketones, this atom-economical² strategy remains limited in application due to a lack of catalysts that can transform a broad range of simple olefins with high regiocontrol.³ Willis and Weller have recently reported a highly efficient rhodium/bisphosphine catalyst for the coupling of β -*S*-substituted aldehydes⁴ with a wide variety of unactivated alkenes.⁵ Despite the frequent use of salicylaldehydes in intermolecular hydroacylation,⁶ however, a method with comparable efficiency, alkene scope, and practicality still remains elusive for this type of aldehyde substrate.^{7,8} Developing such a method would open up a general route to a range of arylketones that could be applied to the synthesis of biologically active polyketide natural products.⁹

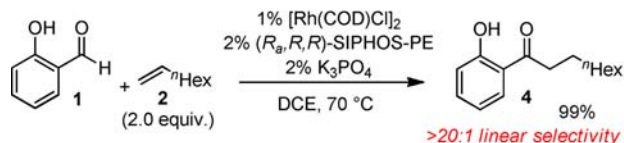
Our group has recently communicated the enantioselective hydroacylation of sulfur-containing alkenes with salicylaldehydes based on a double-chelation approach.^{6h,10} Using chiral phosphoramidite ligand (*R_w*,*R_r*)-SIPHOS-PE,¹¹ homoallylic sulfides such as **2A** could be transformed into the branched arylketone products (**3A**) with high regio- and enantiocontrol (Scheme 1a). This study represented the first example of asymmetric hydroacylation of unactivated olefins and highlighted the unique ability of phosphoramidites in hydroacylation.¹² Given these initial results, we aimed to better understand this catalyst and apply our system to the functionalization of simple olefins, without the need for a directing sulfide or other heteroatom functionality.^{6j,k} In this article, we show that our previously reported rhodium-phosphoramidite catalyst can be used to achieve linear-selective

Scheme 1. Rh-Phosphoramidite Catalyzed Hydroacylation

a) Our initial communication (2010): Sulfide-directed coupling.



b) This study: new scope, application, and mechanistic insight.



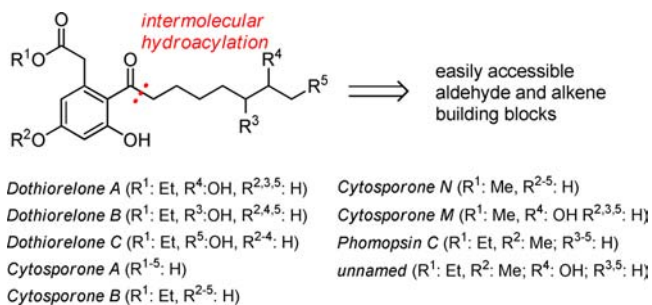
hydroacylation of a wide range of monosubstituted olefins (Scheme 1b). Mechanistic studies show that the chiral ligand (*R_w*,*R_r*)-SIPHOS-PE, although initially used for enantiocontrol in the branched-selective protocol (Scheme 1a), possesses unique stereoelectronic properties that enhance reactivity^{13a-c} and promote regioselectivity^{13d-f} in the challenging linear-selective hydroacylation of simple alkenes (Scheme 1b). In addition to fundamental insights on hydroacylation, our study contributes to the unexpected importance of using chiral ligands to enhance both reactivity and regiocontrol in nonasymmetric transformations.¹³

Received: June 9, 2012

Published: August 31, 2012

Moreover, our catalytic protocol could be applied to the step- and atom-economical total synthesis of eight structurally related octaketides that have been isolated from different endophytic fungi within the past decade (Scheme 2).^{9,14} The majority of

Scheme 2. Natural Products Targeted in This Study



these compounds have not been previously synthesized and limited data is currently available on their biological activity due to the low quantities typically isolated.^{14c} Nevertheless, recent reports have identified octaketide natural product cytosporone B as a promising anticancer therapeutic based on its ability to regulate cell proliferation, differentiation, and apoptosis upstream in a biochemical pathway.¹⁵ Simple structural analogues of cytosporone B have been shown to decrease xenograft tumor growth in vivo,¹⁶ indicating the potential benefit of a synthetic method that allowed the convenient preparation of more complex derivatives.

In principle, all members of this natural product family could be prepared through the coupling of simple 2-hydroxybenzaldehydes with unactivated terminal alkenes (Scheme 2). However, the previously reported hydroacylations by Jun^{7d} and Suemune^{6f} were not applicable to the total synthesis of cytosporone B.¹⁷ Applying Jun's protocol, based on activation of the aldehyde via reversible imine formation, gave no appreciable amount of product in our hands. Suemune's protocol, requiring the use of 40 mol % rhodium catalyst, resulted in formation of the natural product, albeit in 5% yield. These experiments highlight the need for more general and efficient hydroacylation methods.

RESULTS AND DISCUSSION

It occurred to us that the Rh/(*R_w*,*R_r*)-SIPHOS-PE catalyst (Scheme 1a)^{6h} could be effective for the intermolecular hydroacylation of a broader range of alkenes and ultimately be suitable for the total synthesis of octaketide natural products (Scheme 2). We hypothesized that phosphoramidite ligands such as (*R_w*,*R_r*)-SIPHOS-PE that are good π -acceptors and relatively bulky should promote this reaction by decreasing the barrier to reductive elimination, which has been implicated as the turnover-limiting step for related hydroacylations.^{8c,18} To test our hypothesis, we used Rh/(*R_w*,*R_r*)-SIPHOS-PE for the model reaction of salicylaldehyde (**1**) with unactivated alkene **2** and obtained the linear ketone **4** in 90% yield and excellent selectivity (entry 1, Table 1).

Phosphorus-Based Ligands. In light of this initial finding, we evaluated 30 other commercially available phosphorus-based ligands for the transformation of salicylaldehyde (**1**) with 1-octene (**2**) (Table 1 and Table S1 in the Supporting Information (SI)). Phosphoramidite ligands (entries 1–7) were among the few ligands that effectively promoted the transformation. (*R_w*,*R_r*)-SIPHOS-PE gave excellent reactivity

Table 1. Effect of Phosphorus-Based Ligands

Entry	Ligand	Catalyst loading ^a	4+3 (%) ^b	4:3 ^c
1	(<i>R_w</i> , <i>R_r</i>)-SIPHOS-PE	20 mol%	95 (90)	>98:2
2	"	10 mol%	96 (92)	>98:2
3	(<i>R</i>)-SIPHOS	20 mol%	77	95:5
4	"	10 mol%	65 (59)	94:6
5	(<i>R</i>)-MONOPHOS	20 mol%	29	88:12
6	(<i>R,R</i>)-L1	20 mol%	13	92:8
7	(<i>S_w</i> , <i>R_r</i>)-SIPHOS-PE	10 mol%	9	89:11
8	(<i>R</i>)-ShiP	20 mol%	6	90:10
9	(<i>R</i>)-SITCP	20 mol%	14	94:6
10	PPh ₃	20 mol%	79	>98:2
11	"	10 mol%	12	93:7
12	DavePhos	20 mol%	49	>98:2
13	"	10 mol%	12	>98:2

^aThe ratio of rhodium to ligand was 1:1 in each case. ^bNMR yield (internal standard: 1,3,5-trimethoxybenzene); isolated yield in parentheses. ^cRegioisomeric ratio determined by integration of crude ¹H NMR. See Supporting Information, Table S1, for all ligand structures and results obtained with further ligands.

and linear selectivity at both 20 and 10 mol % catalyst loading (entries 1 and 2). Neither less bulky ligand (*R*)-SIPHOS (entries 3 and 4) nor phosphoramidites, derived from a BINOL or biphenyl backbone (entries 5 and 6, respectively), resulted in comparable reactivity or selectivity. Commercially available diastereomer, (*S_w*,*R_r*)-SIPHOS-PE (entry 7),¹¹ furnished the product in low yield and selectivity, indicating a mismatch between the stereogenic elements in this ligand.^{19,20} These results suggest that a synergistic effect between the three stereogenic elements in (*R_w*,*R_r*)-SIPHOS-PE is responsible for the excellent reactivity and regioselectivity observed. Structurally related phosphine or phosphite ligands led to poor reactivity (entries 8 and 9).

The solid state structure of precatalyst complex [Rh(COD)-Cl((*R_w*,*R_r*)-SIPHOS-PE)] (**5**, Figure 1) illustrates the large steric bulk of (*R_w*,*R_r*)-SIPHOS-PE, as well as the intricate spatial arrangement of its stereochemical components (see SI for a crystal structure of mismatched diastereomeric complex [Rh(COD)Cl((*S_w*,*R_r*)-SIPHOS-PE)]).²¹

Finally, monodentate phosphines PPh₃ and DavePhos²² were effective at 20 mol % catalyst loading, but a significant drop in

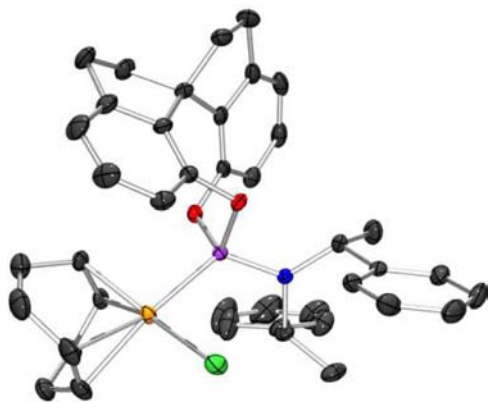
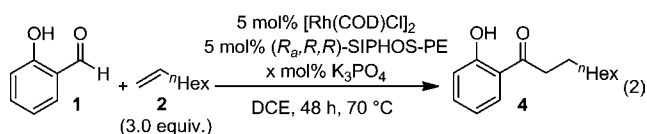


Figure 1. Solid-state structure of catalyst complex 5: $[\text{Rh}(\text{COD})\text{Cl}] \cdot ((R,R,R)\text{-SIPHOS-PE})$. Single crystals were obtained by slow diffusion of hexanes into a CHCl_3 solution. P, purple; O, red; N, blue; Rh, orange; Cl, green; C, black. Key bond lengths (Å) and angles (deg): Rh–P, 2.2614(6); Rh–Cl, 2.3617(5); P–N, 1.6534(19); Cl–Rh–P, 89.70(2); O–P–O, 101.41(8); Rh–P–N, 121.80(7).

reactivity was observed at 10 mol % loading, presumably due to premature catalyst deactivation via decarbonylation (entries 4 and 5).²³ All other Buchwald-type ligands, as well as all surveyed bisphosphine ligands, resulted in poor reactivity (see SI).

Base Stoichiometry. A study on the base/[Rh] ratio revealed that the relative amount of heterogeneous base critically impacts reactivity (Table 2).²⁴ Presumably, the base

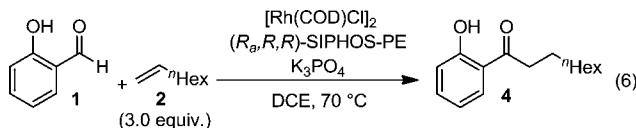
Table 2. Variation of K_3PO_4 /[Rh] Ratio



Entry	mol% K_3PO_4	K_3PO_4 /[Rh] ratio	4+3 (%) ^a	4:3 ^b
1	none	-	0 ^c	n.d.
2	2.5	1:4	31	96:4
3	5	1:2	83 (76)	98:2
4	10	1:1	96 (89)	>98:2
5	20	2:1	22	95:5
6	80	8:1	9	94:6

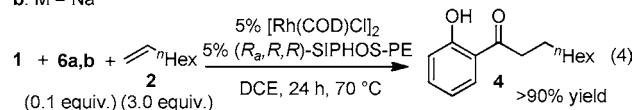
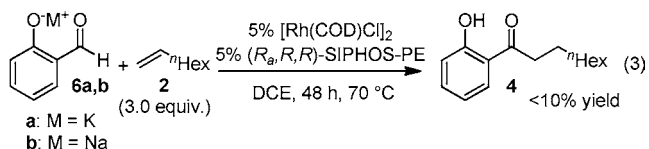
^aNMR yield (internal standard: 1,3,5-trimethoxybenzene); isolated yield in parentheses. ^bRegioisomeric ratio determined by integration of crude ^1H NMR. ^cBased on analysis by GC–MS. n.d.: not determined.

Table 3. Optimization of Rhodium Catalyst Loading



Entry	$[\text{Rh}(\text{COD})\text{Cl}]_2$	$(R,R,R)\text{-SIPHOS-PE}$	K_3PO_4	Scale	Concentration	Reaction time	4 (%) ^a	Ratio 4:3 ^b
1	5 mol%	10 mol%	10 mol%	0.1 mmol	0.1M	24 h	96 (92)	>98:2
2	2.5 mol%	5 mol%	5 mol%	0.1 mmol	0.1M	48 h	93 (87)	>98:2
3	1 mol%	2 mol%	2 mol%	0.5 mmol	1.0M	72 h	quant. (99)	>98:2
4	0.5 mol%	1 mol%	1 mol%	1.0 mmol	1.0M	72 h	75 ^c	>98:2

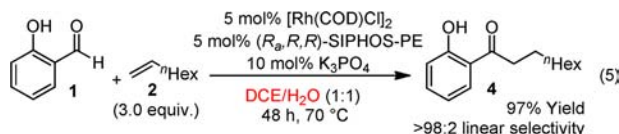
^aNMR yield (internal standard: 1,3,5-trimethoxybenzene); isolated yield in parentheses. ^bRegioisomeric ratio determined by integration of crude ^1H NMR. ^cThe remainder of the mass balance constituted salicylaldehyde (1).



deprotonates salicylaldehyde to make the strongly coordinating phenolate anion,^{6a} which can then undergo oxidative addition onto Rh. Accordingly, we observed no reactivity in the absence of base (entry 1).

However, we observed an increase in yield when the base/[Rh] ratio was increased from 1:4 to 1:1 (entries 2–4). A drastic drop in reactivity was observed when a base/[Rh] ratio of 2:1 or 8:1 was used (entries 5 and 6).

When we submitted the potassium and sodium salts (6) of salicylaldehyde to the reaction conditions, less than 10% yield was obtained in both cases (eq 3). This finding indicates that an excess of 6a relative to rhodium inhibits catalytic turnover (see also Table 2, entry 6). However, when salicylaldehyde (1) was treated with 1-octene (2) in the presence of catalytic amounts of salts 6a or 6b in lieu of K_3PO_4 , excellent reactivity was observed (eq 4). When we investigated a wide range of heterogeneous and homogeneous bases for the reaction of 1 with 2, we found that all soluble bases were completely



ineffective for the transformation (see Table S5 in the SI for details). Mechanistic studies support the notion that excess soluble base promotes catalyst deactivation via decarbonylation processes (vide infra).

Optimizing Solvent and Concentration. A brief study of various rhodium sources revealed $[\text{Rh}(\text{COD})\text{Cl}]_2$ was ideal (see SI, Table S6). Among the chlorinated solvents examined, DCE gave the best reactivity (see SI Table S7 for details). The reaction also proceeded well in tetrahydrofuran, 1,4-dioxane and the renewable solvent,²⁵ 2-methyltetrahydrofuran.²⁶ No significant reactivity was observed in more polar solvents, such as propylene carbonate, or strongly coordinating solvents, such as acetonitrile. The catalytic protocol is also effective in the absence of added solvent (i.e., in neat octene, see SI). The

product was isolated in 97% yield when biphasic conditions (DCE/water, 1:1) were used (eq 5). To the best of our knowledge, this represents the first report of a biphasic aqueous/organic hydroacylation reaction. Separating base and catalyst into two phases minimizes the detrimental effect of excess base on catalytic activity and results in a more robust protocol. We observed 90% yield of product **4** when a 10-fold excess of K_3PO_4 with respect to catalyst was used (in DCE alone this would result in poor yield; refer to Table 2, entry 6).

Finally, we were pleased to find that the reaction proceeded smoothly with only 5 mol % [Rh], provided that an equimolar amount of K_3PO_4 base was used (Table 3, entry 2). A further decrease in catalyst loading, however, necessitated an increase in reaction concentration.²⁷ An isolated yield of 99% was obtained when 2 mol % of rhodium, ligand and base were used at a concentration of 1.0 M (entry 3). When the catalyst loading was decreased to 1 mol % [Rh], 75% yield of product **4** was observed due to incomplete conversion of aldehyde starting material (entry 4).

Aldehyde Scope. With these optimized conditions in hand (1:1:1 ratio of rhodium, ligand and base), we studied the reactivity of other salicylaldehyde derivatives at 5 mol % catalyst loading and 0.4 molar concentration. As shown in Table 4, both

Table 4. Aldehyde Scope

Entry	Aldehyde	t (h)	3 ^{a,b}
1	R: 6-Me (1a)	40	66%
2	R: 5-F (1b)	48	78%
3	R: 5-Cl (1c)	48 ^c	89%
4	R: 5-I (1d)	60 ^c	97%
5	R: 4-OMe (1e)	36	82%
6	R: 4-OH (1f)	5d ^d	95%
7	1g	24	96%
8	1h	48	0%
9	1i	72 ^e	48%

^aIsolated yield. ^bRegioisomeric ratio was >95:5 in all cases (determined by integration of crude ¹H NMR spectrum). ^cFour equivalents of alkene used. ^dSolvent: 2-Me-THF; 2.5 mol % base used. ^eNo base added, 6.0 equiv of alkene used (neat).

sterically hindered (entry 1), as well as electron-deficient (entries 2 and 3) and electron-rich (entries 5 and 6) 2-hydroxybenzaldehydes gave good to excellent yields of the corresponding linear products. 5-Iodosalicylaldehyde (**1d**, entry 4) reacted cleanly—no products indicative of competing protodeiodination or Mizoroki-Heck coupling were observed.

Dihydroxybenzaldehyde (**1f**), which is not soluble in DCE, reacted smoothly in 2-Me-THF (entry 6), and served as a model substrate for the total synthesis of octaketide natural products (vide infra). 2-Hydroxy-1-naphthaldehyde (**1g**) furnished the desired product in excellent yield and regioselectivity (entry 7). A control experiment with 2-

methoxybenzaldehyde (**1h**, entry 8) confirmed that the reaction indeed requires the 2-hydroxy group to proceed. Our method was also effective, however, for 2-(methylthio)benzaldehyde (**1i**), a substrate previously only transformed with cationic rhodium catalysts.^{1,4f,5}

Alkene Scope. Next, we investigated a wide range of monosubstituted alkenes (Table 5). Electron-rich, electron-

Table 5. Alkene Scope

Entry	Alkene	t (h)	4+3 ^a	4:3 ^b
1	2B	70 ^c	93%	>95:5
2	2C	72 ^d	63%	>95:5
3	2D	24	89%	>95:5
4	2E	70 ^c	90%	89:11
5	2F	46	94%	>95:5
6	2G	48	86%	>95:5
7	2H	48	77%	>95:5
8	2I	84	93%	86:14
9	2J	36	98%	89:11 ^f
10	2K	30	77%	88:12
11	2L	24	90%	91:9
12	2M	48 ^e	64%	>95:5
13	2N	36	91%	69:31 ^f
14	2O	24	64%	58:42
15	2P	48	0%	-
16	2Q	48	34%	-
17	2R	29	quant.	63:37

^aCombined isolated yield. ^bRegioisomeric ratio determined by integration of crude ¹H NMR spectrum. ^cFour equivalents of alkene and 10 mol % [Rh] used. ^dFive equivalents of alkene (neat) and 2.5 mol % base used. ^eTen mole percent [Rh] used. ^fThe branched isomer was isolated and an ee of <5% was determined by chiral SFC (see SI). ^gBiphasic reaction conditions (DCE/H₂O, 1:1) were applied.

neutral, as well as electron-deficient alkenes (entries 1–13) displayed good to excellent reactivity under the optimized reaction conditions or slight modifications thereof. Electron-rich vinylsilane **2B** (entry 1), for example, underwent hydroacylation in good yield and with excellent linear regioselectivity. Acrolein diethyl acetal (**2E**, entry 4), not previously reported to undergo hydroacylation, gave 89% yield and 89:11 selectivity. Upon acetal deprotection, this allows for the convenient synthesis of hard-to-access 1,4-ketoaldehydes.

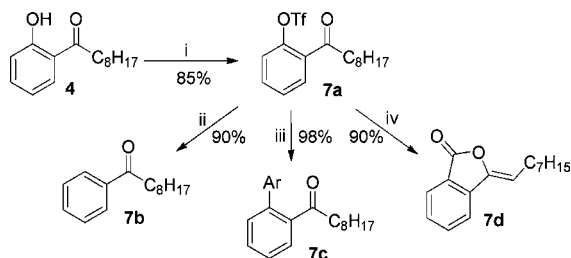
Essential to our proposed natural product syntheses, polar functional groups, as present in alcohol **2H** (entry 7) and

protected amine **2I** (entry 8), were tolerated under the reaction conditions. Styrene **2J** and two representative derivatives **2K** and **2L** (entries 9–11) underwent hydroacylation in good yields and with synthetically useful selectivities. The conventional route toward the corresponding linear reaction products involves a two step aldol condensation/hydrogenation sequence.²⁸ Intermolecular hydroacylation provides a one step protocol to these compounds from inexpensive starting materials. Under biphasic reaction conditions, electron-deficient acrylamide **2M** underwent hydroacylation in 64% yield and excellent linear selectivity (entry 12). Biphasic reaction conditions tend to be superior to standard conditions for strongly chelating alkene substrates (such as **2M**). Acrylate **2N** (entry 13) gave excellent reactivity, yet only modest selectivity.

Terminal alkyne **2O** (entry 14) gave good reactivity, but only poor selectivity. No products of hydroacylation were obtained when conjugated terminal alkyne **2P** (entry 15) was subjected to standard reaction conditions. We observe a deep red color upon addition of base and broad peaks in the ¹H NMR spectrum; substrate **2P** may undergo deprotonation and subsequent polymerization under these reaction conditions. Symmetrical, internal alkyne **2Q** (entry 16) was moderately reactive and resulted in the exclusive formation of the (*E*) product.^{6a} Diene **2R** (entry 17) illustrates two limitations of our method: (i) disubstituted double bonds, as present in 2-octene or compound **2R**, are generally not reactive; (ii) alkenes that can chelate to the Rh-center due to a neighboring double bond or heteroatom can significantly reduce the linear selectivity (in such cases, the regioselectivity is partially controlled by the substrate, not the catalyst; see Scheme 1a).²⁹

Removing or Functionalizing the 2-Hydroxy Group in Hydroacylation Product 4. Encouraged by the relatively broad alkene scope (Table 5), we examined methods to use the 2-hydroxy moiety as a functional handle. As shown in Scheme 3, hydroacylation product **4** can be smoothly transformed into

Scheme 3. Derivatization of Hydroacylation Product **4**^a



^aReaction conditions: (i) Tf₂O (1.5 equiv), pyridine (1.5 equiv), DMAP (0.4 equiv), DCM, 0 °C → RT, 16 h, 85%; (ii) BH₃·Me₂NH (1.05 equiv), K₂CO₃ (1.0 equiv), Pd(PPh₃)₄ (5 mol %), MeCN, 40 °C, 16 h, 90%; (iii) Ar–B(OH)₂ (1.5 equiv), K₂CO₃ (2.5 equiv), Pd(PPh₃)₄ (5 mol %), toluene, reflux, 6 h, 98% (Ar = 4-Et-Ph); (iv) CO (1 atm), Et₃N (2.0 equiv), Pd(OAc)₂ (10 mol %), dppp (10 mol %), DMF, 60 °C, 1 h, 90%.

the corresponding triflate **7a**. Using a method reported by Lipshutz and co-workers, we were able to remove the triflate functionality to afford **7b** in 90% yield without observable reduction of the reactive aromatic ketone.³⁰ The 2-hydroxy functionality in aldehydes **1a–g** can thus be considered a removable directing group.³¹

Triflate **7a** can engage in Pd-catalyzed cross-coupling reactions, as exemplified by the highly efficient Suzuki–Miyaura coupling shown in Scheme 3 (product **7c**). We took advantage

of both the triflate and ketone functionalities present in **7a** to furnish 3-ylidenephthalide **7d** via cyclocarbonylation.³²

Natural Product Synthesis. Having explored the scope of our new hydroacylation method, we turned our attention toward preparing natural products **10a–h** (Table 6). Aldehyde coupling partners **8** were prepared in two steps from commercial materials via Vilsmeier–Haack formylation,³³ followed by AlCl₃ deprotection of the aryl methyl ethers³⁴ (Scheme 4a). Alkene building blocks **9** were either commercially available or could be prepared in one step by copper catalyzed addition of simple Grignard reagents to enantiopure epoxides (Scheme 4b).³⁵

Using our hydroacylation protocol, we prepared eight octaketides (**10a–h**) in good isolated yields (Table 6). Presumably due to a chelation effect, dothiorelone B was obtained in only moderate yield under standard hydroacylation conditions (**10c**, entry 3). Pleasingly, we were able to obtain 86% yield for this product under biphasic reaction conditions (DCE/H₂O). In cases where the reactions proceeded with less than 95:5 linear selectivities, we were able to separate the two regioisomers by chromatography. The reduced linear selectivity in these substrates presumably stems from chelation of the hydroxyl groups on the alkene building blocks to the rhodium catalyst. A ninth natural product, cytosporone A (**10i**, R^{1–5}: H),^{14a} was synthesized from cytosporone B (**10a**) by LiOH-mediated saponification of the ethyl ester (see SI).

This study represents the first total synthesis of compounds **10c**, **10d**, **10f**, **10g**, **10h**, and **10i**.³⁶ While we generally observed good agreement between our spectroscopic data and the data presented in the isolation reports, we found significant deviations in the ¹H and ¹³C NMR data for compound **10f** (see SI for a comparison table). We propose that the material isolated by Huang et al. in 2009^{14d} is not identical to compound **10f**, which we have synthesized and fully characterized as part of this study. Octaketides **10b**, **10c**, **10f**, and **10h** were prepared in enantiopure form, allowing the assignment of the absolute configuration as (*R*) in natural products **10b** and **10h**, based on comparison of [α]_D values (see Table 6). For natural product dothiorelone B (**10c**), the stereochemical assignment was confirmed by an X-ray crystal structure (Figure 2).

The advantages of our synthetic approach include easy access to functionalized terminal alkenes and high functional group tolerance for the C–C bond forming reaction.³⁷ Dothiorelone A, for example, is the only natural product with a hydroxy-substituent on the acyl side chain that has been previously synthesized,^{36c} but the reported synthetic route required 12 linear steps from commercial starting materials. We were able to prepare this compound in three steps in the longest linear sequence (and four steps in total) using an atom-economic intermolecular hydroacylation reaction as the key step.

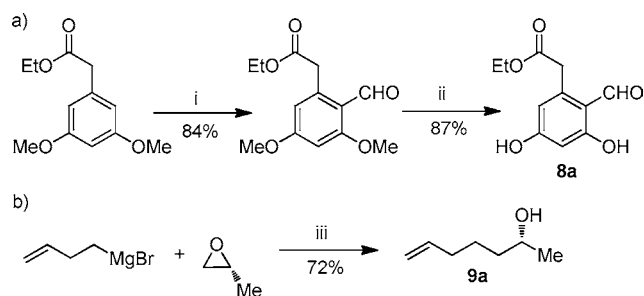
Deuterium Labeling: Insights into Regioselectivity and the Turnover-Limiting Step. To gain insight into the reaction mechanism, we subjected deuterium-labeled salicylaldehyde (*d*-**1** or *h/d*-**1**)³⁸ and selected alkenes to standard reaction conditions for 16–24 h (Table 7). After typical workup, ¹H NMR analysis revealed the deuterium content in residual salicylaldehyde *h/d*-**1**. Both regioisomeric products *h/d*/*d*₁/*d*₂/*d*₃/*d*₄-**3** and *h/d*/*d*₁/*d*₂/*d*₃/*d*₄-**4** were subsequently isolated, and the purified material was analyzed by ¹H and ²H NMR spectroscopy, as well as by high-resolution mass spectrometry.

Table 6. Total Synthesis of Natural Products via Alkene Hydroacylation

Entry	Natural Product	Structure ^a	Isolation	Previous Syntheses	$[\alpha]_D$ lit.	$[\alpha]_D$ found	10 (%) ^b	lin/br ^c
1	cytosporone B	R ¹ : Et (10a)	refs 14a-c, 15	refs 36a,b	-	-	78	93:7
2	dothiorelone A	R ¹ : Et, R ³ : OH (10b)	refs 14b,d	ref 36c	-6, +3.4 (S) ^d	-3.5 (R)	79	83:17
3	dothiorelone B	R ¹ : Et, R ³ : OH (10c)	refs 14b,d,e	-	not reported	-4.0 (R)	59, 86 ^e	>95:5
4	dothiorelone C	R ¹ : Et, R ⁵ : OH (10d)	refs 14b,d	-	-	-	83	87:13
5	phomopsin C	R ¹ : Et, R ² : Me (10e)	refs 14c	ref 36b	-	-	78	>95:5
6	unnamed	R ¹ : Et, R ² : Me, R ⁴ : OH (10f)	refs 14c	-	not reported	-3.3 (R)	79	90:10
7	cytosporone N	R ¹ : Me (10g)	refs 14e	-	-	-	73	94:6
8	cytosporone M	R ¹ : Me, R ³ : OH (10h)	refs 14e	-	-10	-4.0 (R)	73	89:11

^aUnspecified R substituents are H. ^bCombined isolated yield. ^cRegioisomeric ratio determined by integration of crude ¹H NMR spectrum. ^dAn $[\alpha]_D$ of +3.4 was reported for synthetic (S)-dothiorelone A (ref 36c). ^eBiphasic conditions used (1:1 DCE:H₂O). General reaction conditions: [Rh(COD)Cl]₂ (5 mol %), (R_ω,R,R)-SIPHOS-PE (5–10 mol %), K₃PO₄ (5–10 mol %), DCE, 70 °C, 18–72 h. See SI for details.

Scheme 4. Representative Synthesis of Aldehyde and Alkene Building Blocks 8a and 9a^a



^aReaction conditions: (i) DMF (5.0 equiv), POCl₃ (1.2 equiv), RT, 19 h, 84%; (ii) AlCl₃ (10 equiv), DCM, 0 °C → 40 °C, 87%; (iii) CuCN (10 mol %), THF, -78 °C → RT, 14 h, 72%.

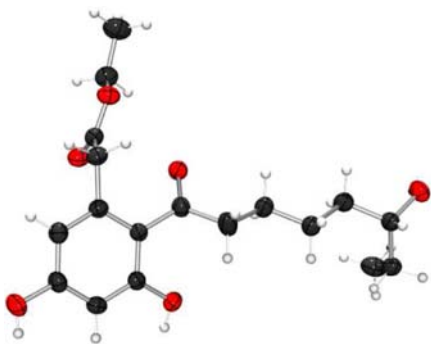


Figure 2. Solid-state structure of octaketide natural product dothiorelone B (**10c**). Single crystals were obtained by slow diffusion of hexanes into a DCE solution. O, red; C, black; H, white.

The mechanistic conclusions derived from these studies are summarized in the catalytic cycle presented in Scheme 5. In agreement with literature reports,^{8c,18} we propose that oxidative addition (step i) and alkene coordination (step ii) are rapid and reversible under the reaction conditions. The magnitude of the kinetic barriers for elemental steps iii-a,b and iv-a,b (Scheme 5) can vary significantly for different types of alkenes (unactivated, activated or chelating), but a general trend is that branched hydride insertion (iii-a) is fast and fully reversible. In contrast to previous reports on olefin hydroacylation,^{8c,18} we propose that linear hydride insertion (iii-b) is fully irreversible for activated

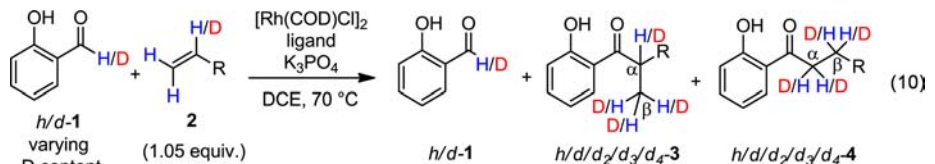
substrates **2J** and **2N** and largely irreversible⁴⁰ for unactivated alkenes such as **2**. In conjunction with our observation of catalytic resting state [Rh(COD)Cl]((R_ω,R,R)-SIPHOS-PE)] (**5**, vide infra), these findings indicate that hydride insertion is turnover-limiting in the linear pathway. These mechanistic studies provide deeper insight into the high regioselectivity observed in our catalytic hydroacylation using Rh/(R_ω,R,R)-SIPHOS-PE.

When 1-octene was subjected to standard conditions (Table 7, entry 1), a deuterium content of ca. 25% was found in residual aldehyde **1** and both the α- and β-positions in product **4**. This observation indicates that the branched hydride insertion (iii-a) is readily occurring and fully reversible under the reaction conditions (see Scheme 5). Reversible insertion to generate the branched intermediate IIIa would lead to incorporation of deuterium into the terminal position of olefin **2**. Subsequent linear deuterioacylation of this olefin would generate ketone **4** with deuterium incorporated at both the α- and β-positions. Because no appreciable quantities of branched product **3** were formed, we conclude that reductive elimination to form ketone **3** (iv-a, Scheme 5) is turnover-limiting in the branched-pathway and relatively slow compared to the turnover-limiting step in the linear pathway (>98:2 linear selectivity observed).

Treating the same substrates with less selective catalyst system Rh/(R)-SIPHOS allowed characterization of both regioisomers **3** and **4** (entry 2). Incorporation of deuterium into both the α- and β-position of product **4** occurred in approximately equal amounts, which provides further support that the branched insertion is reversible for this substrate (iii-a, Scheme 5). In branched product **3**, a small but measurable quantity of deuterium was found in the α-position, indicating that linear hydride insertion (iii-b, Scheme 5) is largely but not fully irreversible.⁴¹ If linear insertion was fully reversible, a deuterium content of 15–20% (statistical scrambling of all exchangeable hydrogen/deuterium atoms) would be expected in the α-position of product **3**.

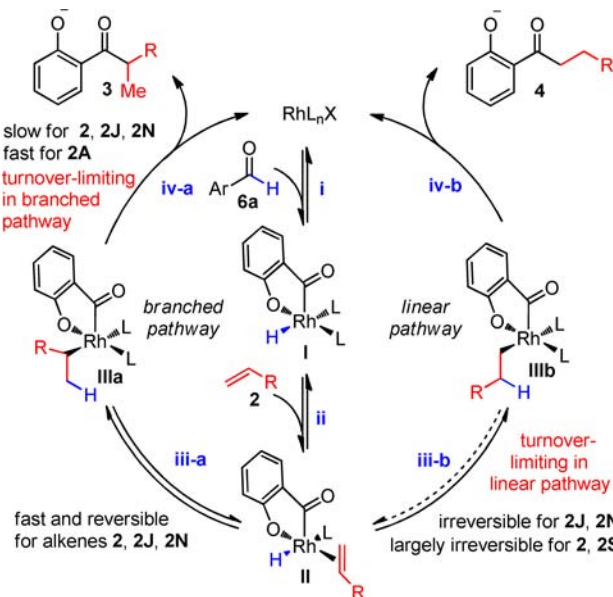
Further support for largely irreversible linear hydride insertion into unactivated olefins is provided by an experiment using deuterium-labeled alkene *d*-**2S** (Table 7, entry 3). When nonlabeled aldehyde **1** was treated with *d*-**2S**,⁴² a nonstatistical deuterium distribution was observed in product **4S** (ca. 50% D found in β, which is higher than the 30% D incorporation expected for statistical scrambling). However, a relatively small

Table 7. Deuterium-Labeling Studies Employing Deuterated Aldehyde or Alkene



Entry	<i>h/d-1</i> ^a	Alkene	Ligand	4:3 ^b Ratio	residual <i>h/d-1</i> ^b	<i>h/d/d2/d3/d4-3</i> ^c	<i>h/d/d2/d3/d4-4</i> ^c
1	100% D	ⁿ Hex (2)	(<i>R_aR_bR_c</i>)-SIPHOS-PE	>98:2	26% D	-	α: 21% D; β: 24% D
2	62% D	ⁿ Hex (2)	(<i>R</i>)-SIPHOS	94:6	21% D	α: ≤6% D; β: 15% D	α: 12% D; β: 16% D
3 ^d	0% D	D C ₉ H ₁₉ (<i>d-2S</i>)	(<i>R_aR_bR_c</i>)-SIPHOS-PE	>98:2	18% D	-	α: ≤5% D; β: 50% D
4	62% D	Ph (2J)	(<i>R_aR_bR_c</i>)-SIPHOS-PE	91:9	25% D	α: 0% D; β: 20% D	α: 15% D; β: 8% D
5	62% D	CO ₂ ^t Bu (2N)	(<i>R_aR_bR_c</i>)-SIPHOS-PE	85:15	24% D	α: 0% D; β: 21% D	α: 19% D; β: 8% D
6 ^e	62% D	SPh (2A)	(<i>R_aR_bR_c</i>)-SIPHOS-PE	<5:95	-	α: 0% D; β: 20% D	-

^aDeuterioenriched salicylaldehyde *h/d-1* (62% D) was conveniently synthesized as shown in Scheme 6b. ^bDetermined by integration of crude ¹H NMR spectrum. ^cDeuterium content of purified 3 and 4 determined by ¹H and ²H NMR spectroscopy, and high-resolution DART mass spectrometry (estimated experimental error: ± 2–3%). Reaction conditions: [Rh(COD)Cl]₂ (5 mol %), ligand (10 mol %), K₃PO₄ (10 mol %), DCE, 70 °C, 16–24 h. ^dThree equivalents of alkene used. ^eDCM was used as solvent; reaction temperature: 30 °C. See SI for further details.

Scheme 5. Proposed Catalytic Cycle^{ab}

^a(i) Oxidative addition; (ii) alkene coordination; (iii) hydride insertion; (iv) reductive elimination. ^bL: (*R_aR_bR_c*)-SIPHOS-PE is likely bound to Rh throughout; the second ligand in intermediates I and III is likely alkene or solvent.³⁹

but measurable quantity of deuterium was found in both residual aldehyde *h/d-1* and in the α-position of product 4S. This result indicates that once intermediate IIIb is formed, only a small fraction of molecules can undergo β-hydride elimination back to intermediate II, explaining the deuterium incorporation into I and into the α-position of 4S (Scheme 5).

Subjecting styrene (2J) and *tert*-butyl acrylate (2N) separately to deuterium-enriched aldehyde *h/d-1* under Rh/(*R_aR_bR_c*)-SIPHOS-PE catalysis gave almost identical deuterium distributions for the two alkenes in both the corresponding branched and linear products (entries 4 and 5). In the branched products 3J and 3N, no measurable deuterium incorporation was observed at the α-position. This result suggests that linear hydride insertion (iii-b, Scheme 5) is irreversible for these types

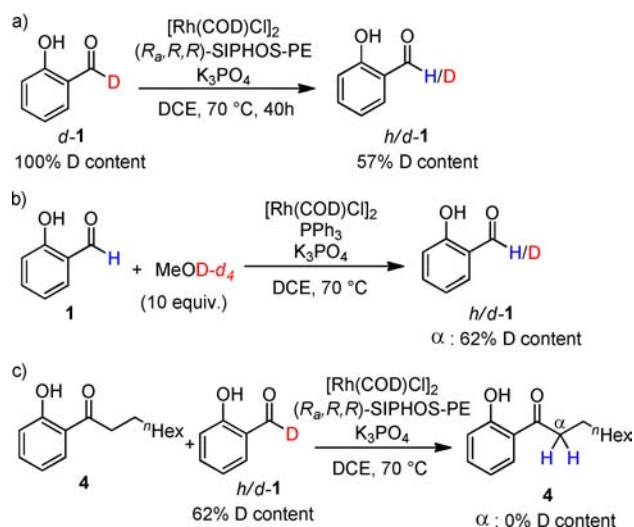
of substrates.⁴³ Higher levels of deuterium were observed in the α-position than in the β-position in linear products 4J and 4N. This result can be explained by a mechanistic scenario in which the branched hydride insertion, iii-a, is fast and steps i and ii (Scheme 5) are fully reversible. At the beginning of this process, alkene substrates with a relatively high terminal deuterium content would be generated, along with aldehyde *h/d-1* with a reduced deuterium content. Once the slower and irreversible linear insertion occurs, lower levels of deuterium are incorporated into the β-position, while the high levels of deuterium in the α-position reflect the high terminal deuterium content of the initially formed alkene.

Homoallylic sulfide 2A was transformed to branched product 3A with no measurable deuterium incorporation in the α-position (entry 6). This observation can be explained by slow and irreversible linear hydride insertion, which is particularly plausible for this substrate where chelation of the sulfur atom to the rhodium catalyst is expected to favor branched over linear hydride insertion through a five-membered rhodacycle.^{6h}

When deuterium-labeled aldehyde *d-1* was subjected to standard reaction conditions in the absence of alkene (Scheme 6a), a decrease of the aldehyde deuterium content to about 57% was found after 40 h. This result indicates that the phenolic hydrogen atoms can slowly exchange with the aldehyde deuterium via rhodium catalysis.⁴⁴ This H/D exchange at the aldehyde does not affect our mechanistic proposal, however, because we derive our conclusions from the relative, not absolute, deuterium content in products 3 and 4. As shown in Scheme 6b, we used this process to achieve a one-step synthesis of deuterium-enriched aldehyde *h/d-1* (62% D) from 1 and deuterated methanol.⁴⁵

In addition, we confirmed that product 4 does not incorporate deuterium at the α-position through a deprotonation-reprotonation mechanism involving exchangeable phenolic D atoms. No measurable deuterium incorporation was found in product 4 after submitting 4 and *h/d-1* to standard reaction conditions (Scheme 6c), indicating that the α-deuterium incorporation presented in Table 7 stems indeed from an organometallic mechanism.

While our observation of turnover-limiting hydride insertion is unprecedented in the olefin hydroacylation literature, Casey

Scheme 6. Control Experiments and Synthesis of Deuterium-Enriched Salicylaldehyde *h/d-1*^a


^aReaction conditions: 10 mol % [Rh], 10 mol % ligand and 10 mol % base. Deuterium content of **1** determined by ¹H NMR spectroscopy. Deuterium content of **4** determined by ¹H and ²H NMR spectroscopy, as well as high-resolution DART mass spectrometry (estimated experimental error: ± 2 –3%).

et al. have made similar mechanistic findings when studying a highly linear-selective rhodium-catalyst for the hydroformylation of 1-hexene.⁴⁶

In Situ NMR Monitoring: Insights into Decarbonylation and the Role of Ligand. Having established a catalytic proposal for the hydroacylation pathway, we sought insight into the decarbonylation side reaction that can drastically limit catalyst turnover. Because of the heterogeneous base required in our catalytic protocol, it was difficult to conduct kinetic studies and establish a precise rate law for hydroacylation or decarbonylation. Therefore, we obtained qualitative kinetic data and aimed to identify catalytic intermediates. In three separate experiments, we varied the relative concentration of substrates **1** and **2** and monitored the reaction progress by ¹H and ³¹P NMR spectroscopy (Figure 3).

Under standard hydroacylation conditions, using 2 equiv of alkene, the reaction followed an exponential time course with no observable induction period, leading to consumption of 96%

of the aldehyde starting material (Figure 3a).⁴⁷ Toward the end of this transformation, ³¹P NMR data indicated the formation of a significant amount of complex **11**, which is tentatively assigned to $[\text{Rh}(\text{CO})\text{Cl}((\text{R}_w, \text{R}_w, \text{R}_w)\text{-SIPHOS-PE})]$ ⁴⁸ on the basis of high-resolution ESI mass spectrometry⁴⁹ and comparison of the obtained ³¹P NMR (162 MHz, DCE, 298 K; $\delta = 126.4$ ppm, $J_{\text{Rh-P}} = 205$ Hz;) and IR (neat; $\nu(\text{CO}) = 1994$ cm⁻¹) spectroscopic data with that of a closely related, known rhodium complex.⁵⁰

When an 8-fold excess of alkene **2** was used, the aldehyde was consumed in only 20 h, despite the lack of stirring (Figure 3b).⁴⁷ A linear kinetic profile was found up to approximately 60% conversion under these conditions. This finding suggests that the potassium salt of salicylaldehyde (**6a**), not salicylaldehyde itself, is the reactive species and that the concentration of **6a** is likely limited by its low solubility in DCE and thus constant for a significant period.⁵¹ After 22 h, analysis of the reaction mixture by ³¹P NMR indicated that a relatively small amount of CO complex **11** was formed (observation of this complex implies reductive decarbonylation of salicylaldehyde). Instead, the major species observed was resting state complex **5** ($[\text{Rh}(\text{COD})\text{Cl}((\text{R}_w, \text{R}_w, \text{R}_w)\text{-SIPHOS-PE})]$).⁵²

In contrast, when an 8-fold excess of aldehyde **1** was used, the transformation proceeded with less than 10% conversion of the starting alkene (Figure 3c). The ³¹P NMR spectrum recorded after 24 h showed that complex **5**, the observed resting state for hydroacylation, had disappeared entirely and CO complex **11** represented the predominant species.⁵³ When monitoring this experiment by ¹H NMR spectroscopy, we observed significant broadening of the phenolic singlets in **1** and **4** at the time when the reaction progress began to slow down. Because this reaction mixture, unlike all others described in this section, eventually turned into a homogeneous mixture, we propose that the observed peak broadening is a result of the gradual solubilization of base **6a** under the reaction conditions.

From these observations, we conclude: (i) excess alkene generally increases the rate of hydroacylation and disfavors decarbonylation; (ii) the precise stoichiometry of base is critical because deprotonated aldehyde **6** is necessary to guarantee high reaction rates, but an excess amount of **6** in solution leads to irreversible catalyst decomposition via reductive decarbonylation. This finding explains the sensitivity of the reaction to the amount and nature of base (Tables 2 and S4), as well as to

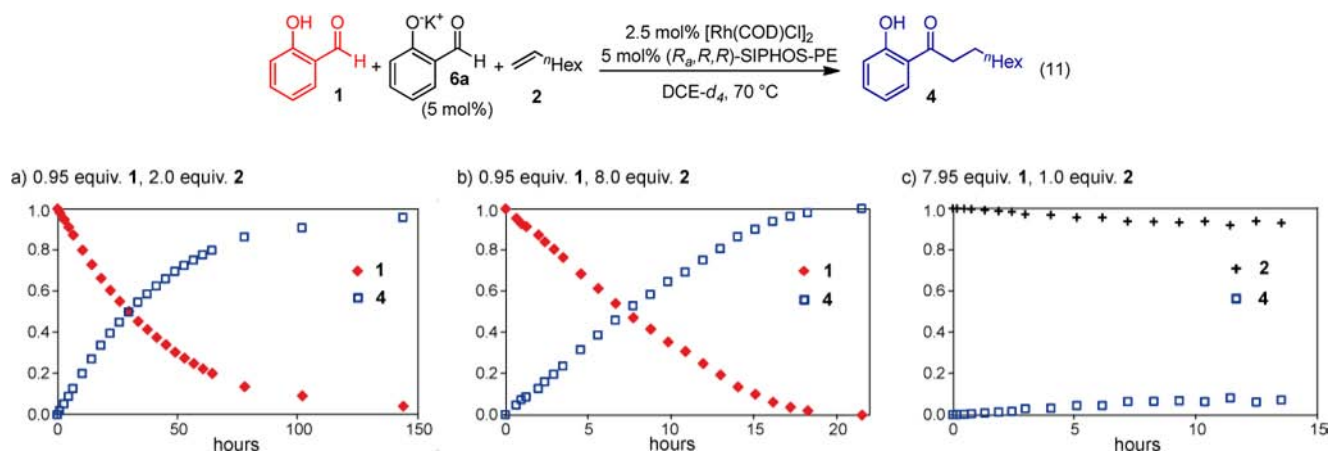
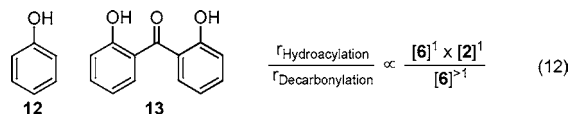


Figure 3. In situ ¹H NMR monitoring (400 MHz, DCE, 343 K) of the reaction of **1** with **2** at different starting material equivalents.

the solvent (Table S6), and provides a rationale for why all studied soluble bases led to low yields.

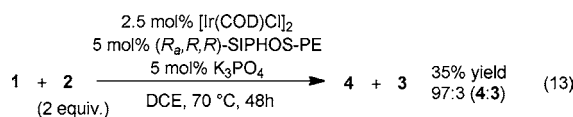
We can only speculate at this point about how excess base triggers catalyst decomposition via reductive decarbonylation. In reactions that resulted in rapid decarbonylation, we generally observed small amounts of phenol (**12**, Chart 1), as well as

Chart 1. Observed Products of Reductive Decarbonylation and Proposed Relative Rate-Dependence



bis(2-hydroxyphenyl)methanone (**13**). We propose that the organometallic pathway leading to this side product is higher than first order in deprotonated salicylaldehyde (**6**), while hydroacylation is likely first order in both **6** and alkene (**2**). Such rate dependences would explain the relatively high propensity for decarbonylation at increased concentrations of **6**, as well as the beneficial effect of excess alkene (Chart 1, eq 12).

Iridium complexes are known to catalyze aldehyde decarbonylation in preference to olefin hydroacylation.^{8a} However, when we replaced precatalyst $[\text{Rh}(\text{COD})\text{Cl}]_2$ with $[\text{Ir}(\text{COD})\text{Cl}]_2$ for the reaction of **1** with **2**, we observed 35% isolated yield for linear hydroacylation product **4**, corresponding to a turnover number of seven. This result indicates that ligand (R_{ω},R,R)-SIPHOS-PE is effective at suppressing competing reductive decarbonylation even when bound to an iridium center. Our results obtained with structurally related ligands (Table 1) indicate that three key factors are responsible for the unique reactivity and selectivity observed with (R_{ω},R,R)-SIPHOS-PE: (i) large steric bulk, (ii) a synergistic effect between the three stereogenic elements, and (iii) the electronic properties of phosphoramidite ligands.^{12a}



Collectively, our mechanistic findings suggest that ligand (R_{ω},R,R)-SIPHOS-PE increases the rate of hydroacylation by decreasing the barrier for reductive elimination toward linear product **4**, while suppressing catalyst decomposition via reductive decarbonylation.

CONCLUSION

We developed a highly efficient method for the linear-selective intermolecular hydroacylation of a wide range of monosubstituted alkenes with salicylaldehyde derivatives. Compared to the previously reported method that allows hydroacylation of **2** with **1**,^{6f} our method stands out due to the broader alkene scope and a 20-fold decrease in rhodium loading. In contrast to most hydroacylation methods reported to date, the catalytic protocol is compatible with environmentally benign solvent, as well as neat or biphasic reaction conditions. We have demonstrated that through a triflate intermediate, the hydroacylation products can be transformed into deoxygenated or more complex building blocks. This catalytic strategy allowed us to prepare eight natural products from the dothiorelone, cytosporone, and phomopsin families, five of which were prepared for the first time. Because of the ease of access to

complex alkene building blocks, our method is ideally suited for the preparation of analogues of anticancer drug candidate cytosporone **B**. Mechanistic studies revealed that for unactivated alkenes, branched hydride insertion is rapid and fully reversible, while linear hydride insertion is largely irreversible. Comparison with a number of related, less effective ligands showed that bulky phosphoramidite (R_{ω},R,R)-SIPHOS-PE is uniquely suited to promote reactivity and regioselectivity in this transformation. Our findings provide insights that will be useful for future catalyst development and ligand design, which will be key to solving the remaining challenges in hydroacylation.

ASSOCIATED CONTENT

Supporting Information

Full synthetic, crystallographic, and characterization details. Crystallographic data have been deposited with the Cambridge Crystallographic Data Centre under CCDC nos. 893320–893322. This material is available free of charge via the Internet at <http://pubs.acs.org>.

AUTHOR INFORMATION

Corresponding Author

dongv@uci.edu

Notes

The authors declare no competing financial interest.

ACKNOWLEDGMENTS

We thank the University of Toronto, Canada Foundation for Innovation, Ontario Research Fund, and NSERC for funding. V.M.D. is grateful for an Alfred P. Sloan Fellowship. M.v.D. is grateful for a postdoctoral fellowship provided by the German National Academy of Sciences Leopoldina (LPDS 2009-43). C.M.L. is grateful for an Ontario Graduate Scholarship. The authors wish to acknowledge the Canadian Foundation for Innovation, project number 19119, and the Ontario MRI for funding of the Centre for Spectroscopic Investigation of Complex Organic Molecules and Polymers. We thank Drs. Burrow and Burns of the CSICOMP NMR facility for assistance with NMR spectroscopy and Dr. Alan Lough for assistance with X-ray crystallography.

REFERENCES

- (1) For a recent review article, see: Willis, M. C. *Chem. Rev.* **2010**, *110*, 725–748.
- (2) (a) Trost, B. M. *Science* **1991**, *254*, 1471–1477. (b) Trost, B. M. *Angew. Chem., Int. Ed.* **1995**, *34*, 259–281.
- (3) To the best of our knowledge, there is only one report of an intermolecular alkene hydroacylation reaction as part of a natural product synthesis: Kim, G.; Lee, E.-j. *Tetrahedron: Asymmetry* **2001**, *12*, 2073–2076.
- (4) For selected studies of alkene hydroacylation relying on S-chelating aldehydes: Willis, M. C.; McNally, S. J.; Beswick, P. J. *Angew. Chem., Int. Ed.* **2004**, *43*, 340–343. (b) Willis, M. C.; Randell-Sly, H. E.; Woodward, R. L.; Currie, G. S. *Org. Lett.* **2005**, *7*, 2249–2251. (c) Willis, M. C.; Woodward, R. L. *J. Am. Chem. Soc.* **2005**, *127*, 18012–18013. (d) Willis, M. C.; Randell-Sly, H. E.; Woodward, R. L.; McNally, S. J.; Currie, G. S. *J. Org. Chem.* **2006**, *71*, 5291–5297. (e) Moxham, G. L.; Randell-Sly, H. E.; Brayshaw, S. K.; Woodward, R. L.; Weller, A. S.; Willis, M. C. *Angew. Chem., Int. Ed.* **2006**, *45*, 7618–7622. (f) Moxham, G. L.; Randell-Sly, H. E.; Brayshaw, S. K.; Weller, A. S.; Willis, M. C. *Chem.—Eur. J.* **2008**, *14*, 8383–8397. (g) Osborne, J. D.; Willis, M. C. *Chem. Commun.* **2008**, 5025–5027. (h) Randell-Sly,

(35) Jastrzebska, I.; Scaglione, J. B.; DeKoster, G. T.; Rath, N. P.; Covey, D. F. *J. Org. Chem.* **2007**, *72*, 4837–4843.

(36) Previous total syntheses: (a) Huang, H.; Zhang, L.; Zhang, X.; Ji, X.; Ding, X.; Shen, X.; Jiang, H.; Liu, H. *Chin. J. Chem.* **2010**, *28*, 1041–1043 (cytosporone B). (b) Yoshida, H.; Morishita, T.; Ohshita, J. *Chem. Lett.* **2010**, *39*, 508–509 (cytosporone B and phomopsin C). (c) Izuchi, Y.; Koshino, H.; Hongo, Y.; Kanomata, N.; Takahashi, S. *Org. Lett.* **2011**, *13*, 3360–3363 (dothiorelone A).

(37) Cytosporone B, and simple derivatives thereof, has been prepared via Friedel–Crafts acylation (ref 16). However, this route is only viable for ketones with nonfunctionalized side chains.

(38) Deuterated salicylaldehyde *d*-1 was synthesized according to ref 6c. Deuterioenriched aldehyde *h/d*-1 was prepared as shown in Scheme 6b.

(39) When monitoring our reactions by ESI mass spectrometry, we did not observe fragments corresponding to two (*R_oR_oR*)-SIPHOS-PE ligands bound to rhodium. For less bulky ligand (*R*)-SIPHOS, we have in contrast observed such fragments. We thus propose that one ligand (*R*)-SIPHOS-PE is bound to rhodium throughout the catalytic cycle, while any vacant sites are occupied by alkene or solvent.

(40) We use the term ‘largely irreversible’ hydride insertion to describe a partially reversible process that within the continuum between a fully reversible and a fully irreversible reaction is relatively close to the irreversible extreme case. In terms of kinetic barriers, our findings imply that from intermediate **IIIb** (Scheme 5) the barrier for β -hydride elimination is approximately 1–2 kcal/mol higher than the barrier for reductive elimination, leading to product **4**. See also ref 46 and: (a) Hartwig, J., Ed.; *Organotransition Metal Chemistry*, University Science Books: Sausalito, CA, 2010; pp 760–762. (b) Casey, C. P.; Martins, S. C.; Fagan, M. A. *J. Am. Chem. Soc.* **2004**, *126*, 5585–5592.

(41) Ligands (*R*)-SIPHOS and (*R_oR_oR*)-SIPHOS-PE differ most significantly in regioselectivity, not reactivity. The results obtained in the deuterium labeling studies using (*R*)-SIPHOS are thus likely applicable to (*R_oR_oR*)-SIPHOS-PE.

(42) 2-Deuteroundec-1-ene (*d*-2S) was prepared according to: Anderson, B. J.; Keith, J. A.; Sigman, M. S. *J. Am. Chem. Soc.* **2010**, *132*, 11872–11874.

(43) An alternative explanation for this result could be that the microscopic reverse of hydride insertion, β -hydride elimination, occurs with stereospecificity. In other words, if deuterium inserts into the double bond, the deuterium atom, and not the geminal hydrogen atom, will undergo the β hydride elimination. Such a scenario could arise when the substrate strongly chelates to the rhodium atom, effectively preventing free rotation around the σ bond. Our experiments are not suitable to rule out such a mechanistic scheme for substrates **2N** and **2A** (alkenes **2** and **2S** cannot chelate to rhodium; **2J** should not be able to bind strongly).

(44) Suemune has reported an analogous loss of deuterium when *d*-1 was subjected to similar conditions (ref 6c). For literature precedence of deuterium/hydrogen scrambling between rhodium hydride complexes and ethanol and a mechanistic proposal for this process see: (a) Detellier, C.; Gelbard, G.; Kagan, H. G. *J. Am. Chem. Soc.* **1978**, *100*, 7556–7561. (b) Stratheede, G.; Given, R. *Can. J. Chem.* **1974**, *52*, 2216–2225.

(45) For previous (multistep) syntheses of deuterated salicylaldehyde (*d*-1), see ref 6c and: (a) Manetsch, R.; Zheng, L.; Reymond, M. T.; Woggon, W.-D.; Reymond, J.-L. *Chem.—Eur. J.* **2004**, *10*, 2487–2506. (b) Moore, J. L.; Silvestri, A. P.; De Alaniz, J. R.; Dirocco, D. A.; Rovis, T. *Org. Lett.* **2011**, *13*, 1742–1745.

(46) Casey, C. P.; Petrovich, L. M. *J. Am. Chem. Soc.* **1995**, *117*, 6007–6014.

(47) Because magnetic stirring was not possible in the NMR spectrometer, the described experiments proceeded significantly slower compared to reactions that were stirred.

(48) Complex **11** could also include an additional ligand that readily dissociates under ESI–MS conditions (e.g., solvent or alkene).

(49) Fragment $[\text{Rh}(\text{CO})(\text{R}_o\text{R}_o\text{R})\text{-SIPHOS-PE}]^+$ was observed by high-resolution ESI⁺–MS (found, 636.1169; calculated, 636.1186).

(50) ³¹P NMR and IR spectroscopic data of complexes **5** (162 MHz, DCE, 298 K; $\delta = 116.1$ ppm, $J_{\text{Rh-P}} = 246$ Hz) and **11** (162 MHz, DCE, 298 K; $\delta = 126.4$ ppm, $J_{\text{Rh-P}} = 205$ Hz; IR (neat): $\nu(\text{CO}) = 1994$ cm^{-1}) is in excellent agreement with data reported for closely related complexes $[\text{Rh}(\text{COD})\text{Cl}(\text{L2})]$ (121.5 MHz, CDCl_3 , RT; $\delta = 112.9$ ppm, $J_{\text{Rh-P}} = 243$ Hz) and $[\text{Rh}(\text{CO})\text{Cl}(\text{L2})_2]$ (121.5 MHz, CDCl_3 , RT; $\delta = 122.3$ ppm, $J_{\text{Rh-P}} = 194$ Hz; IR (neat): $\nu(\text{CO}) = 1983$ cm^{-1}). **L2**: bis(4-methoxyphenyl)dibenzylphosphoramidite. Shejwalkar, P.; Sedinkin, S. L.; Bauer, E. B. *Inorg. Chim. Acta* **2011**, *366*, 209–218.

(51) The observed saturation kinetics could also be explained by the formation of a rhodium–salicylaldehyde complex as a catalytic resting state. Our ³¹P and ESI–MS data do not support such a hypothesis, however. Once the complex $[\text{Rh}(\text{COD})\text{I}^-(\text{R}_o\text{R}_o\text{R})\text{-SIPHOS-PE}]$ is formed, rapid oxidative addition to the corresponding Rh(III)-hydride species seems to occur.

(52) Complex **5** is likely an off-cycle resting state in equilibrium with the corresponding product-bound complex (not observed in large quantity). See also ref 50.

(53) Analysis of the reaction mixture by GCMS confirmed that reductive decarbonylation occurred (i.e., formation of side products **12** and **13**, see Chart 1).